

# Statistical Inference and Visualization in Scale-Space for Spatially Dependent Images

AMY VAUGHAN

College of Business and Public Administration, Drake University, Des Moines, IA 50311, USA

MIKYOUNG JUN

Department of Statistics, Texas A&M University, College Station, TX 77843, USA

CHEOLWOO PARK

Department of Statistics, University of Georgia, Athens, GA 30602, USA

July 15, 2011

## Abstract

SiZer (SIgnificant ZERo crossing of the derivatives) is a graphical scale-space visualization tool that allows for statistical inferences. In this paper we develop a spatial SiZer for finding significant features and conducting goodness-of-fit tests for spatially dependent images. The spatial SiZer utilizes a family of kernel estimates of the image and provides not only exploratory data analysis but also statistical inference with spatial correlation taken into account. It is also capable of comparing the observed image with a specific null model being tested by adjusting the statistical inference using an assumed covariance structure. Pixel locations having statistically significant differences between the image and a given null model are highlighted by arrows. The spatial SiZer is compared with the existing independent SiZer via the analysis of simulated data with and without signal on both planar and spherical domains. We apply the spatial SiZer method to the decadal temperature change over some regions of the Earth.

*Key words:* Goodness-of-fit test, Image data analysis, Kernel smoothing, Scale-space, Spatial correlation, Statistical significance.

# 1 Introduction

SiZer (SIgnificant ZERo crossing of the derivatives) was developed by Chaudhuri and Marron (1999) as an exploratory data analysis tool combined with statistical inferences. It provides a way to look at data so that analysts are able to uncover underlying structure in the data, test the data against underlying assumptions or potential models, and detect any possible anomalies. SiZer is based on a scale-space idea from computer vision, see Lindeberg (1994), where it refers to a family of smooths of a digital image. No particular level of smoothing is regarded as *correct* and each smooth is thought to provide information about the underlying image structure at a particular scale. In SiZer, scale-space is a family of kernel smooths indexed by the bandwidth. Therefore, SiZer is a more advanced version of a basic statistical graphic, such as a plot or chart, that can simultaneously look at data with different scopes.

SiZer is particularly appealing to statisticians for two reasons. First, it considers a wide range of bandwidths to avoid the classical problem of bandwidth selection, which has been a hurdle to the application of smoothers. This allows us to do statistical inference and detect all the information that is available at each individual level of resolution. Second, the target of the SiZer analysis is shifted from the *true underlying curve* to *smoothed versions of the underlying curve*, with the idea that *truth* exists only at each scale. This allows us to avoid a bias problem which occurs in estimating a true underlying function.

Several other versions of SiZer have been developed in recent years. Park et al. (2004) proposed a dependent SiZer that compares the observed time series with an assumed model. Rondonotti et al. (2007) created SiZer for time series, which was later improved by Park et al. (2009a), so that it is able to estimate an autocovariance function in order to detect significant features in a time series. Hannig and Lee (2006) developed a robust version of SiZer which can be used for identifying outliers. Park and Kang (2008) proposed a version of SiZer which can compare multiple curves with independent data based on their differences of smooths and Park et al. (2009b) introduced a SiZer that puts forth a method for comparing two (or more) time series. Park et al. (2010) studied a SiZer which targets the quantile composition of the data instead of the mean structure. In addition, various Bayesian versions of SiZer have also been proposed. These include Erästö and Holmström (2005), Godtlielsen and Oigard (2005), Oigard et al. (2006) and Erästö and Holmström (2007). Note that all of these tools are restricted to one dimensional data, and thus they are not readily applicable to image data in a higher dimension.

In two dimensions, Ganguli and Wand (2007) studied additive modeling for generalized linear models, and Godtlielsen et al. (2002) and Duong et al. (2008) studied multivariate kernel estimation in scale-space. Godtlielsen et al. (2004) proposed what they refer to as  $S^3$ , Significance in Scale-Space, in a regression setting that analyzes image data. Since they assume the errors are independent, we call  $S^3$  the *independent SiZer* in this paper. They state two main challenges of analyzing two dimensional data in scale-space: statistical inference and visualization. In one dimension, statistical inference is based on the derivatives of a curve that have statistically significant increases and decreases, and the scale-space is viewed as an overlay of curves. Instead, for two dimensions Godtlielsen et al. (2002) and Godtlielsen et al. (2004) use partial derivatives, or gradients for statistical inference and introduce a movie version that shows the progression through various bandwidths. This tool is useful for finding meaningful structure in a given image, but it has its limitations due to the independence assumption.

Image data, or spatial data, are commonly observed with spatial dependence structures and we need to take the spatial dependence into account when we do inference on the mean structure. Figure 1 shows the decadal temperature change for 1980–1999 over the area around America and the Himalayan region (see Section 4.1 for more details on this data). The interest here is to detect subregions with statistically significant temperature changes. Like most of the environmental variables, the temperature variable usually exhibits strong spatial dependence and sometimes its dependence structure is quite complex (such as *nonstationary*). For this data set, since we consider the decadal temperature change, the covariance structure may not be as complicated as the temperature variable itself, but there still should be strong spatial dependence in the data. In fact, using the coded scale along the right vertical axis of each map, Figure 1 shows that neighboring pixels are quite correlated. Shen et al. (2002) analyzed a similar data set to detect statistically significant changes in the decadal temperature averages over some parts of America and they used a method called enhanced false discovery rate. Their method does consider the spatial dependence structure of the field.

In this paper, we propose a two dimensional SiZer that improves the independent SiZer by taking the spatial correlation structure into account in image analysis. The proposed method takes the noisy image data and finds significant features compared with a given spatial model. It is also useful to assess models being considered as possible candidates to explain the image well. Although there exists some work for goodness-of-fit tests for spatial point processes (Diggle, 1979)

and spectral densities (Crujeiras et al., 2010), there has not been much work on goodness-of-fit test tools for spatial models. Therefore, the spatial SiZer can provide informative analysis with visualization for a vast range of statistical problems.

Section 2 reviews spatial correlation models and provides details on the proposed spatial version of SiZer. Section 3 tests the spatial SiZer and compares it with the independent SiZer using simulated examples. This study is conducted in both planar and spherical domains and the simulated fields are with and without a signal. In Section 4 we illustrate the usefulness of the proposed method in the problem of detecting the decadal temperature change over some subregions of the Earth. Finally, we discuss extensions of the proposed method in Section 5.

## 2 Methodology

We first review some parametric covariance models for spatial random fields in Section 2.1 and then introduce the proposed SiZer method in Section 2.2.

### 2.1 Models for spatial dependence

Consider data sets that are observed in a spatial domain,  $D \subset \mathbb{R}^d$ . Let us denote a random field by  $Z(\mathbf{s})$  indexed by spatial location  $\mathbf{s} \in D$ . The process  $Z(\mathbf{s})$  may exhibit spatial dependence, similar to time series where the correlation between different time points must be taken into account. In observing  $\{Z(\mathbf{s}_1), \dots, Z(\mathbf{s}_n)\}$  at spatial locations  $\{\mathbf{s}_1, \dots, \mathbf{s}_n\}$ , one of the key issues is how to model the covariance structure of the process  $Z$  across space.

In modeling the covariance structure of a spatial process, we often make some simplifying assumptions. Consider a random field  $\{Z(\mathbf{s}) : \mathbf{s} \in D\}$ . Suppose that the mean  $E\{Z(\mathbf{s})\}$  and the covariance  $C(\mathbf{s}_1, \mathbf{s}_2) = \text{Cov}\{Z(\mathbf{s}_1), Z(\mathbf{s}_2)\}$  exist and are finite for all  $\mathbf{s}, \mathbf{s}_1, \mathbf{s}_2 \in D$ . In general, without any simplifying assumptions, the covariance structure is nonstationary in the sense that  $\text{Cov}\{Z(\mathbf{s}_1), Z(\mathbf{s}_2)\}$  should depend on both  $\mathbf{s}_1$  and  $\mathbf{s}_2$ . We say the process is (*weakly*) *stationary* if the covariance only depends on the difference between the two locations, that is, there exists an appropriate function  $C_1$  such that  $C_1(\mathbf{s}_1 - \mathbf{s}_2) = \text{Cov}\{Z(\mathbf{s}_1), Z(\mathbf{s}_2)\}$  for all  $\mathbf{s}_1, \mathbf{s}_2$ . Furthermore, we say the process is (*weakly*) *isotropic*, if for a suitable function  $C_2$ ,  $C_2(\|\mathbf{s}_1 - \mathbf{s}_2\|) = \text{Cov}\{Z(\mathbf{s}_1), Z(\mathbf{s}_2)\}$ , that is, the covariance only depends on the distance between the two locations. Here  $\|\cdot\|$  denotes the Euclidean distance, but sometimes we need to use a different metric for some spatial domains

(see the last paragraph of this section). Examples of commonly used isotropic covariance functions are the *Gaussian* function,  $C_2(x) = a \exp(-x^2/b^2)$ , the *exponential* function,  $C_2(x) = a \exp(-x/b)$ , and the Matérn function given by

$$C_2(x) = a(x/b)^\nu \mathcal{K}_\nu(x/b). \quad (2.1)$$

The function  $C_2$  is defined on the domain  $[0, \infty)$  and it needs to be *positive definite* on the domain to be a suitable covariance function for any random process. The parameter  $a > 0$  is called the *sill* and it determines the overall level of covariance. For the Gaussian and exponential functions,  $a$  gives the variance of the process at any location and for the Matérn function,  $a \cdot 2^{\nu-1} \Gamma(\nu)$  gives the variance of the process under the parameterization in (2.1). The parameter  $b > 0$  is called the *spatial range* and it determines how far the spatial correlation lasts. For a Matérn covariance function, we have an additional parameter, *smoothness*,  $\nu > 0$ , which determines the smoothness of the process. The function  $\mathcal{K}_\nu$  is the modified Bessel function. The smoothness parameter,  $\nu$ , gives greater flexibility to the covariance structure compared to Gaussian or exponential functions. In fact, Gaussian and exponential models are special cases of the Matérn model in that when  $\nu = \infty$ , the Matérn model is the same as the Gaussian model and when  $\nu = 0.5$ , it is the same as the exponential model. Note that the stationarity or isotropy assumption requires that the mean should be constant over the entire domain. That is, we require  $E\{Z(\mathbf{s})\} = \mu$  for all  $\mathbf{s} \in D$ . However, for the SiZer problem, our goal is to detect the mean structure and thus we cannot assume any structure on the mean of the random field. This difficulty poses a fundamental identifiability problem of the mean and (co)variance and we will discuss this issue further in Section 4.2.

If the process is defined on a planar domain, that is, if  $D \subset \mathbb{R}^2$ , then we simply use the Euclidean distance in evaluating the covariance using (2.1). However, if the process is defined on a spherical domain, which is the case for many of environmental data sets, the distance in (2.1) needs to be the *chordal* distance to have the Matérn model positive definite on the surface of the sphere for all smoothness parameter values (see Jun and Stein (2007) for further discussion). The chordal distance between the two locations on the surface of a sphere,  $(L_1, l_1)$  and  $(L_2, l_2)$  for  $L_1, L_2$  latitudes and  $l_1, l_2$  longitudes, is evaluated by

$$ch(L_1, L_2, l_1 - l_2) = 2R \left\{ \sin^2 \left( \frac{L_1 - L_2}{2} \right) + \cos L_1 \cos L_2 \sin^2 \left( \frac{l_1 - l_2}{2} \right) \right\}^{1/2}, \quad (2.2)$$

where  $R$  is the radius of the sphere. The distances for the data in Sections 3.2 and 4 are calculated using (2.2), while the distance in Section 3.1 is the usual Euclidean distance in  $\mathbb{R}^2$ .

## 2.2 Spatial SiZer

We build the spatial SiZer by extending the independent SiZer from the i.i.d setting to the spatially correlated case. We illustrate the proposed method under the setting and notations of Godtlielsen et al. (2004). The statistical model that underlies the spatial SiZer is

$$Y_{i,j} = s(i, j) + \epsilon_{i,j},$$

where  $i = 1, \dots, n$  and  $j = 1, \dots, m$  index pixel locations,  $s$  represents the underlying deterministic signal, and the  $\epsilon_{i,j}$ 's have mean zero and dependent correlation structure. We assume the covariance structure is isotropic, that is,  $\text{Cov}(\epsilon_{i,j}, \epsilon_{i',j'}) = C_2(d_{(i,j),(i',j')})$ , where  $d_{(i,j),(i',j')}$  is the distance between the two points,  $(i, j)$  and  $(i', j')$ , and  $C_2$  is an isotropic covariance function. Note that the independent SiZer (Godtlielsen et al., 2004) assumes the  $\epsilon_{i,j}$ 's to be independent errors.

The estimates of the signal  $s$  in scale-space are simply Gaussian smooths indexed by the bandwidth (see Jones and Wand (1995) for example); that is, discrete two-dimensional convolutions of a spherically symmetric Gaussian density with the data. One can use two different bandwidths for two different directions  $(i, j)$ , but we use the same bandwidth  $h$  for simplicity. The estimates are denoted as

$$\hat{s}_h(i, j) = \sum_{i'=1}^n \sum_{j'=1}^m Y_{i',j'} K_h(i - i', j - j'),$$

or in matrix notation

$$\hat{\underline{s}}_h = \underline{K}_h * \underline{Y}$$

where  $*$  denotes bivariate discrete convolution,  $\underline{Y} = Y_{i,j}$  for  $i = 1, \dots, n$  and  $j = 1, \dots, m$ ,  $\underline{K}_h = K_h(i, j)$ . Higdon (2002) provided some examples of bivariate kernels including Gaussian and spherical kernels. In this paper we use the bivariate Gaussian kernels. In presenting the SiZer results graphically we let the off diagonal elements of the  $2 \times 2$  covariance matrix in the bivariate Gaussian kernels zero and the diagonal elements equal. This reduces to the product of two univariate kernels,

$$K_h(i, j) = K_h(i)K_h(j),$$

for  $i = (1 - n), \dots, (n - 1)$  and  $j = (1 - m), \dots, (m - 1)$  with

$$K_h(i) = \frac{\exp(-(i/h)^2/2)}{\sum_{i'=1-n}^{n-1} \exp(-(i'/h)^2/2)}.$$

Godtliebsen et al. (2004) suggested to subtract the mean of the  $Y_{i,j}$  before smoothing to overcome the boundary effects due to a result of averaging in zeros from outside the image. Hence,

$$\hat{\underline{s}}_h = A(\underline{Y}) + \underline{K}_h * (\underline{Y} - A(\underline{Y})),$$

where  $A$  is the matrix operator which returns the constant matrix whose common entries are the average of the entries of its matrix argument.

Another consideration is the number of points that should be inside each kernel window, where the effective sample size here is given as

$$\underline{ESS} = (\underline{K}_h * \underline{1}) / (K_h(0, 0)).$$

Here  $\underline{1}$  is the  $n$  by  $m$  matrix having a one in each entry. Using the Binomial rule,  $ESS(i, j) < 5$  indicates the region where the data are sparse for inference. To make  $S^3$  inferences simultaneously across location, Godtliebsen et al. (2004) used an average effective sample size of

$$ESS_2 = \left( \sum_{i=1}^n \sum_{j=1}^m ESS(i, j) \right) / (nm).$$

To adjust  $ESS_2$  for spatially correlated images, we borrow an idea from Rondonotti et al. (2007); the amount of information about the signal available in correlated data is not the same as the amount of information in independent data. The patterns in positively correlated errors behave closely to high frequency signal components, which appear in a family of smooths for a wide range of bandwidths. On the contrary, a family of smooths changes less as a function of the bandwidth in negatively correlated errors due to the tendency of alternating up and down of such errors. Therefore, positively (negatively) correlated data contain less (more, respectively) information about the signal than independent data. Using statistical information ideas, a simple measure of information in the data is provided by the ratio

$$I = \sqrt{\frac{\sum_{i=1}^n \sum_{j=1}^m \sigma_{i,j}^2}{Var(\sum_{i=1}^n \sum_{j=1}^m Y_{i,j})}},$$

where  $V(\epsilon_{i,j} = \sigma_{i,j}^2)$  and

$$Var \left( \sum_{i=1}^n \sum_{j=1}^m Y_{i,j} \right) = \sum_{i=1}^n \sum_{j=1}^m \sum_{i'=1}^n \sum_{j'=1}^m C_2(d_{(i,j),(i',j')}).$$

Using the information  $I$ , which reflects the type and the magnitude of the correlation structure, the modified effective sample size ( $MESS$ ) is given as

$$MESS = I \times ESS_2.$$

Note that for independent data,  $I = 1$ , which induces  $MESS = ESS_2$ .

$MESS$  is used to calculate the approximate number of independent averages

$$\ell = \frac{nm}{(MESS)}. \quad (2.3)$$

For statistical inference of SiZer, let us consider that the norm of the gradient of the underlying signal  $s$  at any given  $(i, j)$  location is

$$G(s) = [(s_1)^2 + (s_2)^2]^{1/2},$$

where  $s_1$  (and  $s_2$ ) is the partial derivative in the vertical (and horizontal) direction. Then, the corresponding estimate of the gradient in scale-space is

$$\hat{G}_h(s) = [(\hat{s}_{h,1})^2 + (\hat{s}_{h,2})^2]^{1/2},$$

where the partial derivatives are estimated by

$$\hat{s}_{h,1} = \underline{K}_{h,1} * \underline{Y}, \quad \hat{s}_{h,2} = \underline{K}_{h,2} * \underline{Y},$$

where  $K_{h,1}(i, j) = K'_h(i)K_h(j)$ ,  $K_{h,2}(i, j) = K_h(i)K'_h(j)$ , and  $K'_h(i) = (-i/h)K_h(i)$ . The gradient version of the SiZer flags pixels with arrows as significant when  $\hat{G}_h(s)$  is higher than the noise level, rejecting a null hypothesis of the form

$$H_0 : G_h(s) = 0.$$

For the independent SiZer, the null distribution of this test is based on the bivariate Gaussian distribution

$$\begin{pmatrix} \hat{s}_{h,1} \\ \hat{s}_{h,2} \end{pmatrix} \sim N \left( \begin{pmatrix} 0 \\ 0 \end{pmatrix}, \begin{pmatrix} \tau_1^2 & \tau_{12}^2 \\ \tau_{12}^2 & \tau_2^2 \end{pmatrix} \right),$$

which is exact if the noise terms  $\epsilon_{i,j}$  have a Gaussian distribution or follow the Central Limit Theorem (Godtliebsen et al., 2004). By the assumption of independence,  $\tau_{12}^2 \approx 0$ . The usefulness of the independent SiZer, however, is diminished if the image is spatially dependent. Due to the

assumption of independent errors, significant features found by the SiZer may be simply artifacts of the natural dependence inherent to the spatially dependent data (see Figure 5(c) as an example). This motivates the need to properly incorporate dependence into the SiZer analysis.

For the spatial SiZer,  $\tau_{12}^2$  is different from zero and the correlation should be accounted for in estimating  $\tau_1^2$  and  $\tau_2^2$ . Therefore, the variance for the partial derivative in the vertical direction, indexed by 1, is

$$\begin{aligned}
\hat{\tau}_1^2 &= \text{Var}(\hat{s}_{h,1}(i, j)) \\
&= \text{Cov} \left( \sum_{i'=1}^n \sum_{j'=1}^m Y_{i',j'} K_{h,1}(i-i', j-j'), \sum_{i''=1}^n \sum_{j''=1}^m Y_{i'',j''} K_{h,1}(i-i'', j-j'') \right) \\
&= \sum_{i'=1}^n \sum_{j'=1}^m \sum_{i''=1}^n \sum_{j''=1}^m K_{h,1}(i-i', j-j') K_{h,1}(i-i'', j-j'') \text{Cov}(Y_{i',j'}, Y_{i'',j''}) \\
&= \sum_{i'=1}^n \sum_{j'=1}^m \sum_{i''=1}^n \sum_{j''=1}^m K_{h,1}(i-i', j-j') K_{h,1}(i-i'', j-j'') C_2(d_{(i',j'),(i'',j'')}).
\end{aligned}$$

The variance in the horizontal direction is given similarly. The covariance between the partial derivatives in the horizontal and vertical directions is given by

$$\begin{aligned}
\hat{\tau}_{12}^2 &= \text{Cov}(\hat{s}_{h,1}, \hat{s}_{h,2}) \\
&= \sum_{i'=1}^n \sum_{j'=1}^m \sum_{i''=1}^n \sum_{j''=1}^m K_{h,1}(i-i', j-j') K_{h,2}(i-i'', j-j'') C_2(d_{(i',j'),(i'',j'')}).
\end{aligned}$$

Here,  $C_2$  can be modeled through a parametric model as explained in Section 2.1. Once these pieces are computed, they are put together to form the covariance matrix

$$\hat{\Sigma} = \begin{pmatrix} \hat{\tau}_1^2 & \hat{\tau}_{12}^2 \\ \hat{\tau}_{12}^2 & \hat{\tau}_2^2 \end{pmatrix}$$

and it leads to the resulting distribution that can be seen as

$$\begin{pmatrix} \hat{\tau}_1^2 & \hat{\tau}_{12}^2 \\ \hat{\tau}_{12}^2 & \hat{\tau}_2^2 \end{pmatrix}^{-1/2} \begin{pmatrix} \hat{s}_{h,1} \\ \hat{s}_{h,2} \end{pmatrix} = \begin{pmatrix} \hat{t}_{h,1} \\ \hat{t}_{h,2} \end{pmatrix} \sim N \left( \begin{pmatrix} 0 \\ 0 \end{pmatrix}, \begin{pmatrix} 1 & 0 \\ 0 & 1 \end{pmatrix} \right).$$

The sum of the squares of these two test statistics results in

$$\hat{t}_{h,1}^2 + \hat{t}_{h,2}^2 \sim \chi_2^2(\alpha'),$$

and thus the null hypothesis  $H_0$  is rejected for those pixels which have values

$$\hat{t}_{h,1}^2 + \hat{t}_{h,2}^2 > q_{\chi_2^2}(\alpha'). \tag{2.4}$$

Here  $\alpha'$  is the adjusted significance level that achieves the nominal level of  $\alpha$ . The nominal level of  $\alpha$  used in all of the numerical examples in this paper is  $\alpha=0.05$ . Doing an approximation based on the number of independent blocks,  $\ell$  in (2.3), we define

$$q_{\chi^2_2}(\alpha') = -2 \log(1 - (1 - \alpha)^{1/\ell}). \quad (2.5)$$

as the quantile for determining significance. Note that the independent SiZer utilizes the different quantile because  $\ell$  is defined using  $ESS_2$  which does not take the correlation into account.

For pixels whose null hypothesis is rejected by (2.4), we determine that pixel location to have a gradient significantly higher than those of its surrounding area. To denote this significance, we follow the visualization suggested by Godtliebsen et al. (2004), which draws an arrow in that gradient direction using the corresponding vertical and horizontal direction vector  $(\hat{s}_{h,1}, \hat{s}_{h,2})$ . A statistically significant extreme is therefore surrounded by a ring of significant gradient arrows pointing towards the peak or valley (see Figure 3(a) as an example).

As noted in (2.4), statistical inference depends on the smoothing level  $h$ . A fundamental idea of SiZer is to use all levels of resolution of the image instead of selecting the best one, and thus a series of images (or a movie version) indexed by the bandwidth is presented in SiZer analysis. For small bandwidths the images still contain a substantial noise component, which can lead to not very clearly defined outlines of the images and few arrows that appear to indicate statistically significant features. As the bandwidth gets large, these images show a blurring of the outlines of the images and many structures marked as significant, which is not particularly useful, since features of interest are typically not visible at this scale. Some slice choice in between therefore typically reveals important features of the image and we choose two bandwidths ( $h = 2, 4$ ) to visualize SiZer analysis in the next two sections to save space.

### 3 Simulation results

We compare the spatial SiZer proposed in this paper with the original independent SiZer in a planar domain ( $\mathbb{R}^2$ ) as well as a spherical domain (an approximation of the surface of the Earth). For each domain, we generate the error process through Gaussian random fields with the covariance structure from the Matérn function given in (2.1). As mentioned at the end of Section 2.1, for the spherical domain, we need to use the chordal distance of the two points on the surface of the sphere

given in (2.2) to get a valid covariance model. We repeat the SiZer analysis many times and show representative images in this section as we obtain similar results.

For the spherical domain case, we also present the proposed spatial SiZer analysis result when the covariance structure is misspecified. We present the case for both the data with and without the signal.

### 3.1 Planar domain

In the simulation, we generate a signal of image from the following equation for  $i = 1, \dots, n$  and  $j = 1, \dots, m$

$$s(i, j) = 10 \left[ \cos \left( \frac{180 \times 10}{\pi} \left( i - \frac{n}{2} \right) \right) \cdot \cos \left( \frac{180 \times 10}{\pi} \left( j - \frac{m}{2} \right) \right) \right]_+. \quad (3.1)$$

Here,  $n = 30$  is the length in the vertical direction,  $m = 30$  is the length in the horizontal direction, and  $(\cdot)_+$  indicates the positive part of the function (the negative pieces are set to zero). For the covariance structure, we try eight different combinations of parameter values in (2.1), that is,  $a = 5, 10$ ,  $b = 2, 5$ , and  $\nu = 0.5, 1.5$ . Figure 2 (a) displays the original signal in (3.1). To save space, we report only two cases below, (i)  $a = 5, b = 2, \nu = 0.5$  and (ii)  $a = 10, b = 5, \nu = 1.5$ , but other results are similar.

In Figure 3, it can be seen that the spatial SiZer highlights the most prominent feature of interest cleanly for both  $h = 2$  and  $4$  as the arrows of the spatial SiZer point inward toward the center of the mode. Also, it captures all four small features at the corners. The independent SiZer, although its arrows are angled for convergence at the center of the mode, marking its peak as the significant focal point, has such a vast number of spurious pixels that they cover almost the entire map. Thus, this independent SiZer provides an inaccurate representation of the amount of actual trend that lies within the image. Figure 4 shows a similar result except that the small features at the corners are not well captured by the spatial SiZer for  $h = 4$ . However, this does demonstrate the fact that when a large value of a smoothing parameter is used, often only large scale features are revealed with this macroscopic vision. Similarly, when a small value of a smoothing parameter is used, more small scale features are identified with this microscopic vision. In summary, Figures 3 and 4 show that the spatial SiZer outperforms the independent SiZer since it correctly identifies important features and also reduces number of spuriously highlighted pixels.

In the next two figures, we use the same error structure as above, but remove the signal.

Therefore, a properly working SiZer tool should find no features. In Figures 5 and 6, the spatial SiZer’s performance is exemplary, with not a single pixel erroneously highlighted. The bright and dark pixels seen in the image are known to be sampling artifacts and are correctly not highlighted as significant in the spatial SiZer. This can also be viewed as a goodness-of-fit test, that is the image can be modeled by the Matérn function with the given parameters. However, in the independent SiZer there are numerous arrows converging to focus on some of both the bright and dark areas of the map. These abundant arrows often seem to point at nothing or fail to completely enclose the convergence point of its arrows. This shows that the independent SiZer has denoted that there is a significant trend present at all of these random locations, where in fact there is not. These cases demonstrate that the spatial SiZer can correctly differentiate between the dependent error structure and true significant trend, while the independent SiZer cannot.

### 3.2 Spherical domain

We consider the domain on the surface of the Earth and create a  $30 \times 30$  regularly spaced domain over latitude range  $11^\circ$  S to  $47^\circ$  S and longitude range  $148.75^\circ$  E to  $221.25^\circ$  E. This particular subregion is chosen arbitrarily and thus in the figures with results, we do not overlay the world map. The mean and covariance structures are similar to those in Section 3.1 except that for the data with signal, we use

$$s(L, l) = 4 \exp \left[ -\sqrt{\{(l - 160)^2 + (L - 30)^2\}/30} \right] + 4 \exp \left[ -\sqrt{\{(l/2 - 100)^2 + L^2\}/10} \right], \quad (3.2)$$

for  $L$  latitude and  $l$  longitude (in degrees). For the covariance parameters, we use  $a = 0.03, 0.08$ ,  $b = 500, 1000$ , and  $\nu = 0.5, 1.5$ . Note here that the unit for the spatial distance is miles, that is, the radius of the Earth,  $R$ , in (2.2) is in miles. Figure 2 (b) displays the original signal in (3.2).

To save space we only report two cases below, (i)  $a = 0.03, b = 1000, \nu = 0.5$  and (ii)  $a = 0.08, b = 500, \nu = 1.5$ , but other results are similar. In Figures 7 and 8, when  $h = 2$ , the independent SiZer again has numerous spurious pixels around the true features and in the upper right hand corner of the image, that appear to point at nothing and never converge. For  $h = 4$ , the image in both SiZers becomes oversmoothed and the arrows can barely be separated enough to mark the two modes. With the independent SiZer in Figure 7 (d) the map even has a pixel at every possible location of the image, thus providing no case of differentiating signal from noise. This is also nearly the case in Figure 8 (d), when no real informational inference is given when almost every pixel

in the map has been deemed significant. Figures 7 and 8 again show the superior performance of the spatial SiZer to the independent SiZer because it finds the true features (see Figure 8 (a)) and greatly reduces the number of spuriously highlighted pixels. This example, however, shows that the spatial SiZer also has room for improvement because it flags some spurious pixels as significant (see Figure 7 (a)). As noted in Section 2.2, using a new quantile which takes the spatial correlation into account is one way of improving the current tool.

We also conduct goodness-of-fit tests for both SiZers by removing the signal and generating only noise. In Figures 9 and 10 the spatial SiZer has not a single highlighted pixel, thus it does not show any significant features. This clearly confirms that the data are consistent with the error generated from the Matérn function with the given parameters. As to the opposite conclusion, the independent SiZer flags varied bright and dark pixels as significant all over the image. In Figures 9 (d) and 10 (d), when  $h = 4$ , almost all of the image is highlighted again, blurring the arrows together which have declared significant trend, but are actually merely sampling artifacts. This clearly implies that the image cannot be modeled by an independent Gaussian model.

Lastly, we test the sensitivity of the spatial SiZer method on the covariance structure since in many real applications the true covariance structure is unknown. Figure 11 shows the SiZer analysis when true covariance structure is given by Matérn function with  $a = 0.08, b = 500, \nu = 1.5$  but we assume Matérn covariance structure with  $a = 0.08, b = 500, \nu = 0.5$ . In other words, the true covariance structure is much smoother than the assumed covariance structure (note that the assumed covariance structure is the same as the exponential covariance function). In both cases of with and without the signal, the result shows that the proposed SiZer correctly identifies the location of the signal. We also test the SiZer method when the data are generated using a spherical covariance function,  $C_2(x) = 0.03\{1 - \frac{3}{2}(\frac{x}{500}) + \frac{1}{2}(\frac{x}{500})^3\}\mathbf{1}_{(x < 500)}$  with the same signal as above. Figure 12 presents the result when we assume the Matérn covariance function with  $a = 0.026, b = 155.08, \nu = 0.87$ , instead of the true spherical covariance structure. The parameter values used are the maximum likelihood estimates from the Matérn covariance function. Figure 12(a) shows that the proposed SiZer using the incorrect covariance structure gives a reasonable result although it tends to flag more spurious pixels. This may imply that the Matérn covariance function is flexible enough that as long as we use the covariance parameter estimates from the data, the spatial SiZer produces accurate analyses.

The simulations in Sections 3.1 and 3.2 demonstrate that the spatial SiZer performs superior to

the independent SiZer as it correctly identifies significant features, limits the number of spuriously highlighted pixels, and successfully conducts goodness-of-fit tests for various types of errors from the Matérn covariance function.

## 4 Application

In this section, we apply the methodology developed in Section 2 to the problem of detecting the decadal temperature change over some regions of the Earth. One of the regions that we analyze is similarly studied by Shen et al. (2002) and we compare our result with theirs in Section 4.3.

### 4.1 Data

To study the climate change specifically induced by the anthropogenic emissions, various organizations throughout the world are developing climate models under the coordination of the Intergovernmental Panel on Climate Change (IPCC). There are 20+ state-of-the-art climate models being developed worldwide and Jun et al. (2008) analyzed some of these models, some outputs of which are used in this paper. Shen et al. (2002) dealt with the output from an older version of the climate model called CSM, developed by the National Center for Atmospheric Research (NCAR). In this paper, we use the outputs of two climate models, one, CCSM3 (this is the model's IPCC I.D.), developed by NCAR, and the other, GFDL-CM2.0, developed by NOAA/Geophysical Fluid Dynamics Lab. The CCSM3 model is a newer and more advanced version of CSM, to the extent that they are almost two completely different models. Similar to Shen et al. (2002), we will also take a look at the time period of 1980–1999. The climate model outputs are given in monthly averages. The spatial grid resolution of the CCSM3 is  $256 \times 128$  and that of the GFDL-CM2.0 is  $144 \times 90$ .

Our interest is in the average temperature change between the periods 1980–1989 and 1990–1999, in a spatial domain containing some parts of North and South America as well as a domain around the Himalayan area. The American region gives an image of size  $46 \times 57$  when we take a look with the CCSM3 model and a  $33 \times 33$  size pixel image with GFDL-CM2.0. The Himalayan area is a  $41 \times 52$  with CCSM3 and a  $30 \times 30$  pixel image with the GFDL-CM2.0 model. We aim to detect whether the surface temperature has changed over these two decades and we also want to identify the regions of change using the spatial SiZer, if any such change exists. Also, we will compare the

results on these climate changes between the two climate models, CCSM3 and GFDL-CM2.0, as well as comparing our result from using the CCSM3 model with the CSM results presented in Shen et al. (2002).

Figure 1 shows the decadal difference of surface temperature (unit: K) over the two regions with the two climate models. To evaluate the level of surface temperature change, we compare the variation in hue of adjacent pixels. Those with shades that are closer in terms of levels of brightness and darkness are more similar than those that are not. Using this as our guide, we can see that the patterns and values of the temperature changes for the American region are quite similar between the two models. Note that the pattern of temperature change is smoother over the ocean as expected. However, the pattern of temperature changes over the Himalayan area from the two models are quite different. The two maps seem to use different colors for similar regions. For example, GFDL-CM2.0 implies noticeable temperature decrease over East Africa but CCSM3 does not suggest clear temperature change over that region. On the other hand, CCSM3 suggests apparent temperature decrease over the region with latitude range  $30^\circ$  N to  $55^\circ$  N and longitude range  $50^\circ$  E to  $80^\circ$  E but it is not the case with the GFDL-CM2.0 output. Our goal is to test the statistical significance of all of these patterns.

## 4.2 Covariance estimation

It is common to model a spatial random field with a fixed mean structure through certain covariates and the covariance structure through some parametric covariance functions. The parameters in the mean as well as in the covariance function can be estimated through the maximum likelihood estimation method or weighted least squares method. To improve the covariance parameter estimation in the maximum likelihood method, we use the restricted maximum likelihood (REML) method. For detailed discussion on advantages and disadvantages of these methods, see Cressie (1993). For our analysis, we need to estimate covariance parameters to implement the spatial SiZer developed in Section 2.2.

Since we cannot assume any structure on the mean part of the process under our setting, the estimation of the covariance parameters can be problematic. A similar (but simpler) problem arises for a time series with temporal dependence, and Park et al. (2009a) used time differencing as an attempt to remove the mean part and then applied the weighted least squares method to estimate an autocorrelation function. They also used a regularization technique to improve the estimation.

If the mean structure for the spatial process is close to being constant (nonzero) or is slowly and smoothly varying, then we may also consider spatial differencing: for each pixel, we subtract the average of neighboring pixels to get rid of the mean structure. Let  $\mathbf{Z} = \{Z(\mathbf{s}_1), \dots, Z(\mathbf{s}_n)\}$  be the vector of the data (suppose we have  $n$  spatial locations total) and  $\mathbf{K}$  be the appropriate differencing matrix. Then similarly to the REML method, we can maximize the likelihood of  $\mathbf{KZ}$  to get the estimates for the covariance parameters.

In our analysis, we estimate the covariance parameters using a maximum likelihood estimation method with and without spatial differencing. Interestingly, the covariance parameter estimates by these two approaches for both data sets are fairly close. In the next subsection, we present results using the covariance parameter estimates without spatial differencing (but we subtract the spatial average from the original data to make the overall mean zero).

### 4.3 Result

Using the MLE approach to estimation, the values of the covariance parameters for the Matérn function for the CCSM3 model outputs are  $a = 0.024$ ,  $b = 261.04$ ,  $\nu = 1.33$  for the region over America and  $a = 0.027$ ,  $b = 213.74$ ,  $\nu = 1.27$  for the region around the Himalayan area. Using the GFDL-CM2.0 model, the MLE values of the covariance parameters for the Matérn function for the outputs are  $a = 0.052$ ,  $b = 425.82$ ,  $\nu = 1.12$  for the region over America and  $a = 0.055$ ,  $b = 532.32$ ,  $\nu = 0.83$  for the region around the Himalayan area. The parameter estimates with spatial differencing are quite similar for both cases under the same model. This similarity between the fits with and without spatial differencing gives us confidence that the true mean structure is not too far from being a constant, and thus the mean structure may not affect the covariance parameter estimates significantly. Note that the parameter estimates for the two regions are quite similar for each of the two climate models.

We now show the results of both SiZer methods portrayed through Figures 13 - 16. For both the American data in Figures 13 and 15 and the Himalayan data in Figures 14 and 16, big differences between the two climate models can be seen from the spatial SiZer plots. If we take a look at the spatial SiZer plots using the GFDL-CM2.0 model output in Figures 13 and 14, since there are no arrows, this implies that there is no significant temperature change present. To the contrary, in the spatial SiZer plots at both bandwidths utilizing the CCSM3 model output in Figures 15 and 16, it can be seen that there are several regions with significant temperature changes denoted by

the arrows. Note that different  $h$  values for the spatial SiZer give quite different results for CCSM3 in Figure 15. Shen et al. (2002) also reported quite significant temperature changes in several regions over the America, which is somewhat consistent with our CCSM3 results. The fact that the independent SiZer determines that there are significant changes at many places on maps from both climate model outputs over both regions indicates that the independent SiZer cannot accurately account for the spatial dependence that is present in this temperature change data.

## 5 Conclusion and future work

In this paper, we develop a spatial SiZer, which takes into account the spatial dependence structure in an image. Through simulation results, we demonstrate that the spatial SiZer works well while the independent SiZer flags spurious signals. Our application result shows that CCSM3 climate model suggests significant decadal temperature changes over the regions of America and Himalayan area, while GFDL-CM2.0 climate model suggests no significant temperature change over the same regions.

We have two suggestions for future work. First, one can develop a SiZer which is capable of comparing several images. This is particularly useful when different algorithms are applied to an image and one wants to compare the output images. Another example is when one is interested in finding statistically significant resolution dependent differences among several noisy images. Comparison between two images is usually made numerically with, for example, Mean Squared Error, which simply incorporates tallies over the two images of corresponding pixel differences, regardless of position or intensity. But, it does not always give convincing results and no statistical inference is involved. Moreover, statistical comparison of several images has not been widely studied. Recently, Hölmstrom and Pasanen (2009) use a Bayesian scale-space approach to capture the scale dependent differences in two noisy images of the same scene taken at two different instants of time.

Second, a further step would be to construct a SiZer for data with spatial-temporal dependence. For example, in functional Magnetic Resonance Imaging (fMRI) studies, data are collected in a sequence of three dimensional images over time. One scanned image is composed of  $64 \times 64$  pixels and this scan process continues for a certain time period, which typically results in a couple of hundred images. Thus, each pixel is a time series with a couple of hundred time points. The simultaneous exploration of spatial and temporal correlations in fMRI data can be achieved by

combining SiZer for time series and spatial SiZer, and constructing a three dimensional SiZer for spatial-temporal data. There are various parametric spatio-temporal covariance models available to model the fMRI data. Furthermore, visualization of high dimensional statistical inference will be yet another nontrivial component of the proposed future research.

## Acknowledgments

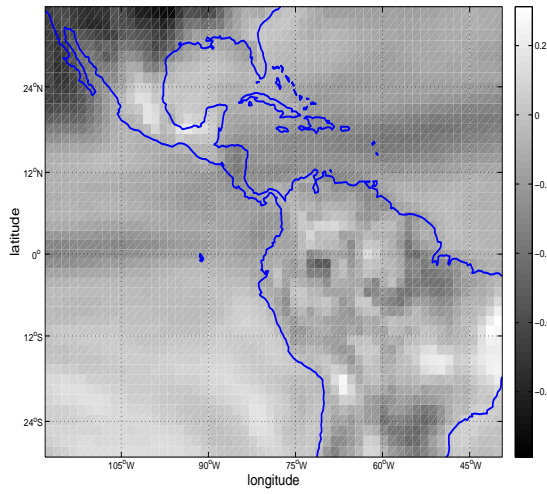
This work is part of the first author's dissertation. Mikyoung Jun acknowledges support from NSF grants ATM-0620624 and DMS-0906532. Mikyoung Jun's research is partially supported by Award No. KUS-C1-016-04, made by King Abdullah University of Science and Technology (KAUST). The authors acknowledge the modeling groups for making their simulations available for analysis, the Program for Climate Model Diagnosis and Intercomparison (PCMDI) for collecting and archiving the CMIP3 model output, and the World Climate Research Programme (WCRP)'s Working Group on Coupled Modelling (WGCM) for organizing the model data analysis activity. The WCRP CMIP3 multi-model dataset is supported by the Office of Science, U.S. Department of Energy.

## References

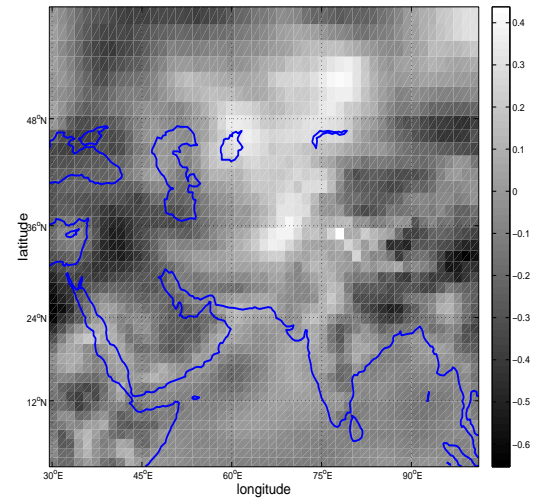
- Chaudhuri, P. and Marron, J. S. (1999). SiZer for exploration of structures in curves. *Journal of the American Statistical Association*, 94:807–823.
- Cressie, N. (1993). *Statistics for Spatial Data*. Wiley, NY.
- Crujeiras, R. M., Fernández-Casal, R., and González-Manteiga, W. (2010). Goodness-of-fit tests for the spatial spectral density. *Stoch Environ Res Risk Assess*, 24:67–79.
- Diggle, P. J. (1979). On parameter estimation and goodness-of-fit testing for spatial point patterns. *Biometrics*, 35:87–101.
- Duong, T., Cowling, A., Koch, I., and Wand, M. P. (2008). Feature Significance for Multivariate Kernel Density Estimation. *Computational Statistics and Data Analysis*, 52:4225–4242.
- Erästö, P. and Holmström, L. (2005). Bayesian multiscale smoothing for making inferences about features in scatter plots. *Journal of Computational and Graphical Statistics*, 14:569–589.

- Erästö, P. and Holmström, L. (2007). Bayesian analysis of features in a scatter plot with dependent observations and errors in predictors. *Journal of Statistical Computation and Simulation*, 77:421–434.
- Ganguli, B. and Wand, M. P. (2007). Feature significance in generalized additive models. *Statistics and Computing*, 17:179–192.
- Godtlielsen, F., Marron, J. S., and Chaudhuri, P. (2002). Significance in scale space for bivariate density estimation. *Journal of Computational and Graphical Statistics*, 11:1–21.
- Godtlielsen, F., Marron, J. S., and Chaudhuri, P. (2004). Statistical Significance of Features in Digital Images. *Image and Vision Computing*, 22:1093–1104.
- Godtlielsen, F. and Oigard, T. A. (2005). A visual display device for significant features in complicated signals. *Computational Statistics and Data Analysis*, 48:317–343.
- Hannig, J. and Lee, T. (2006). Robust SiZer for exploration of regression structures and outlier detection. *Journal of Computational & Graphical Statistics*, 15:101–117.
- Higdon, D. (2002). Space and space-time modeling using process convolutions. In *Quantitative Methods for Current Environmental Issues (C. Anderson, et al. eds)*, pages 37–54. Springer, London.
- Hölmstrom, L. and Pasanen, L. (2009). Bayesian scale space analysis of differences in images. *Submitted*.
- Jones, M. and Wand, M. (1995). *Kernel Smoothing*. Chapman & Hall, London.
- Jun, M., Knutti, R., and Nychka, D. W. (2008). Spatial analysis to quantify numerical model bias and dependence: How many climate models are there? *Journal of the American Statistical Association*, 103:934–947.
- Jun, M. and Stein, M. L. (2007). An approach to producing space-time covariance functions on spheres. *Technometrics*, 49:468–479.
- Lindeberg, T. (1994). *Scale-Space Theory in Computer Vision*. Kluwer, Boston.

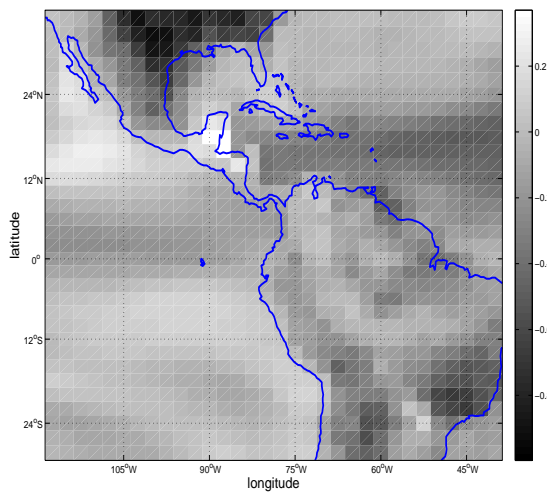
- Oigard, T. A., Rue, H., and Godtlielsen, F. (2006). Bayesian multiscale analysis for time series data. *Computational Statistics and Data Analysis*, 51:1719–1730.
- Park, C., Hannig, J., and Kang, K. (2009a). Improved SiZer for time series. *Statistica Sinica*, 19:1511–1530.
- Park, C. and Kang, K. (2008). SiZer analysis for the comparison of regression curves. *Computational Statistics and Data Analysis*, 52:3954–3970.
- Park, C., Lee, T., and Hannig, J. (2010). Multiscale exploratory analysis of regression quantiles using quantile SiZer. *Journal of Computational and Graphical Statistics*, 19:497–513.
- Park, C., Marron, J. S., and Rondonotti, V. (2004). Dependent SiZer: goodness of fit tests for time series models. *Journal of Applied Statistics*, 31:999–1017.
- Park, C., Vaughan, A., Hannig, J., and Kang, K. (2009b). Sizer analysis for the comparison of time series. *Journal of Statistical Planning and Inference*, 139:3974–3988.
- Rondonotti, V., Marron, J. S., and Park, C. (2007). SiZer for time series: a new approach to the analysis of trends. *Electronic Journal of Statistics*, 1:268–289.
- Shen, X., Huang, H.-C., and Cressie, N. (2002). Nonparametric hypothesis testing for a spatial signal. *Journal of the American Statistical Association*, 97:1122–1140.



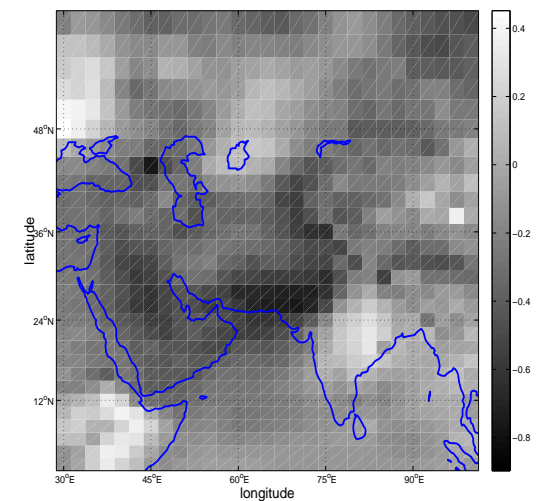
(a) North and South America (CCSM3)



(b) Himalayan area (CCSM3)

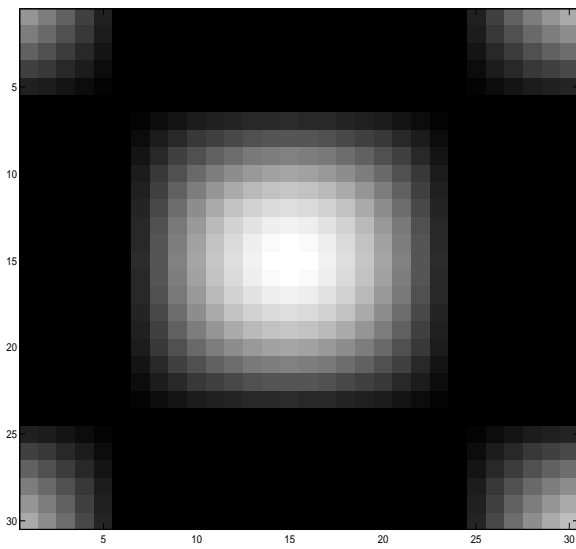


(c) North and South America (GFDL-CM2.0)

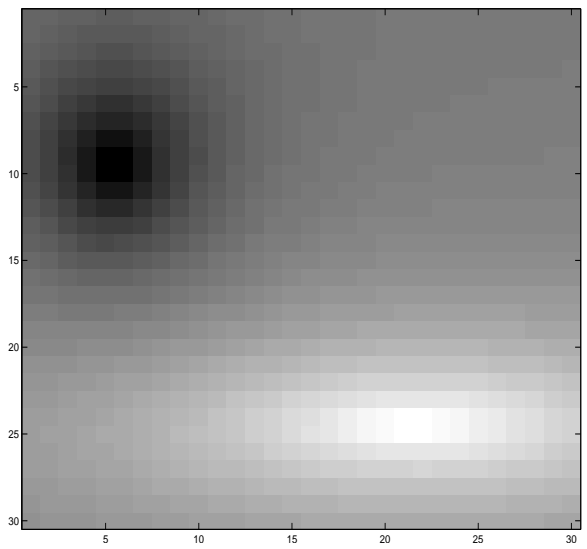


(d) Himalaya area (GFDL-CM2.0)

Figure 1: Decadal temperature change for the time period of 1980–1999 over (a) and (c) parts of North and South America, and (b) and (d) region around Himalayan area. Two climate models are used: CCSM3 for (a) and (b), and GFDL-CM2.0 for (c) and (d). The unit is K.

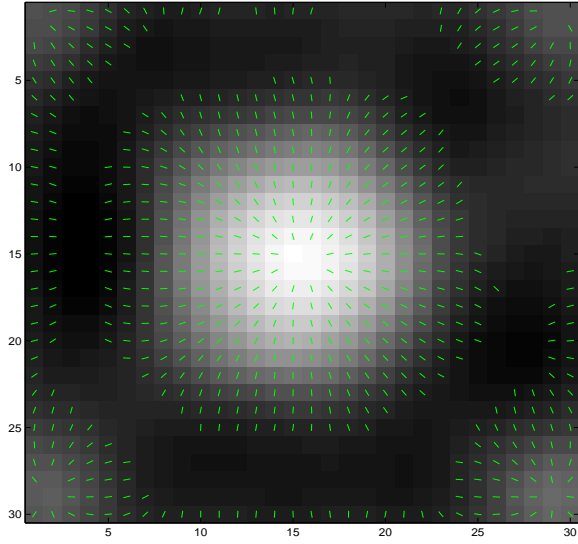


(a) Signal for a planar domain

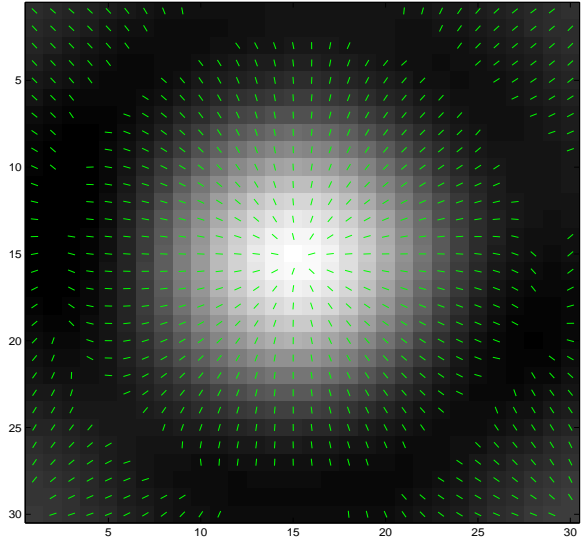


(b) Signal for a spherical domain

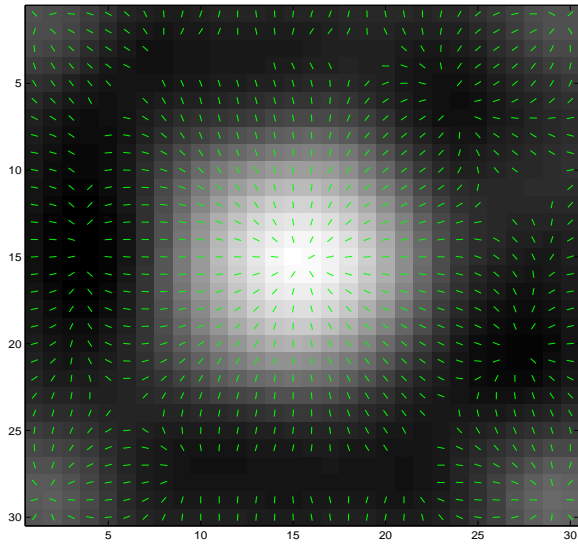
Figure 2: Original signals for planar and spherical domains



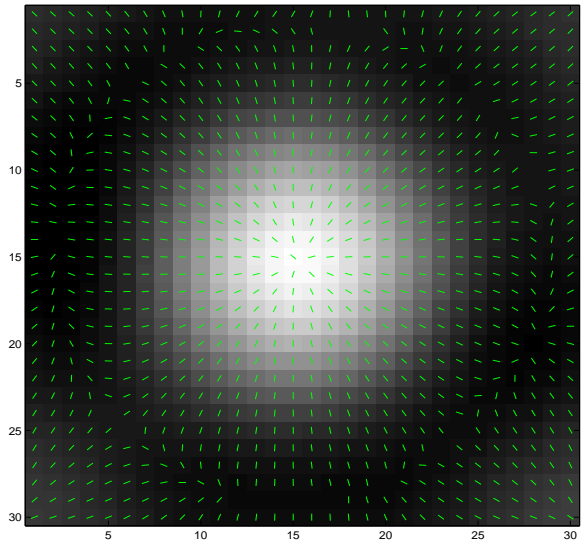
(a) Spatial ( $h = 2$ )



(b) Spatial ( $h = 4$ )

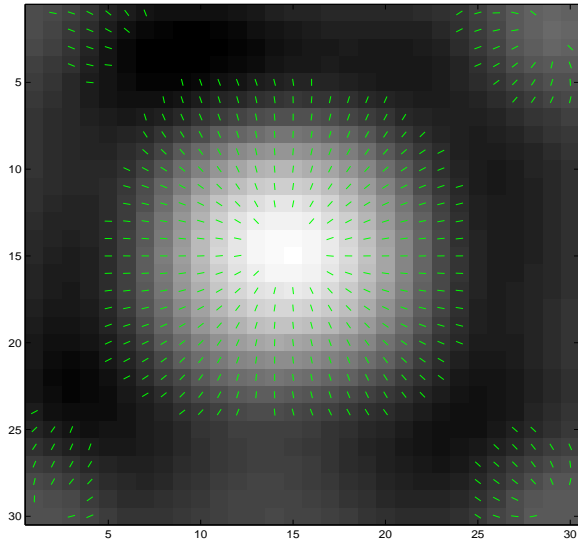


(c) Independent ( $h = 2$ )

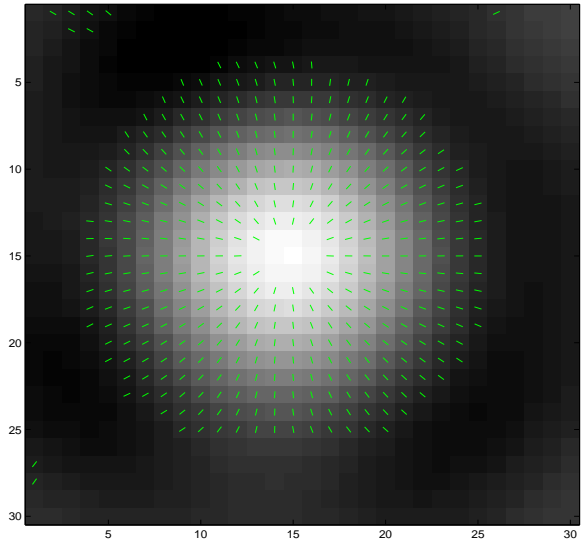


(d) Independent ( $h = 4$ )

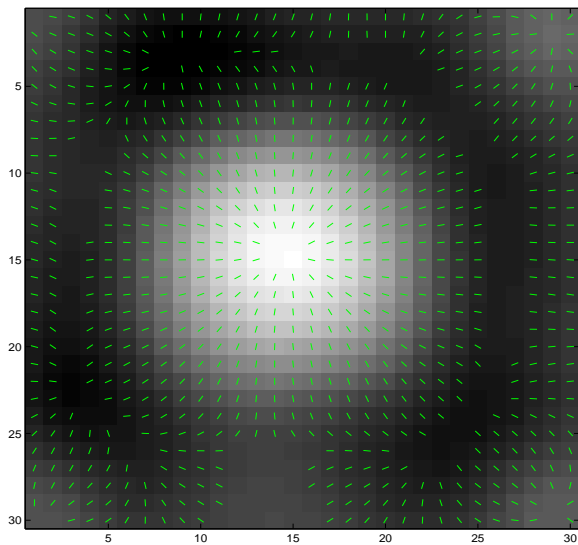
Figure 3: Signal plus Matérn covariance with  $a = 5, b = 2, \nu = 0.5$  on a planar domain



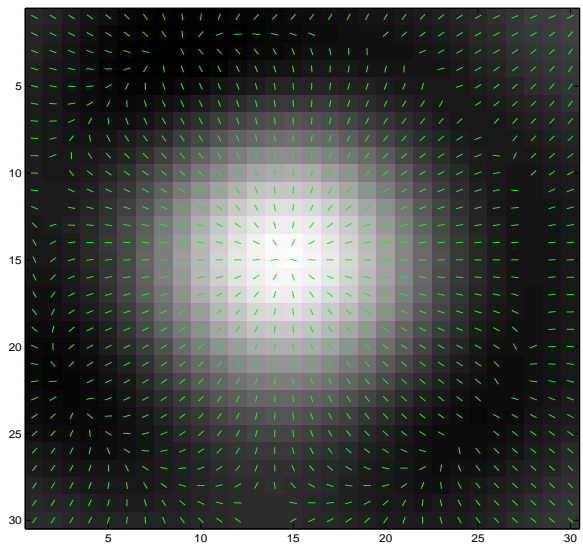
(a) Spatial ( $h = 2$ )



(b) Spatial ( $h = 4$ )

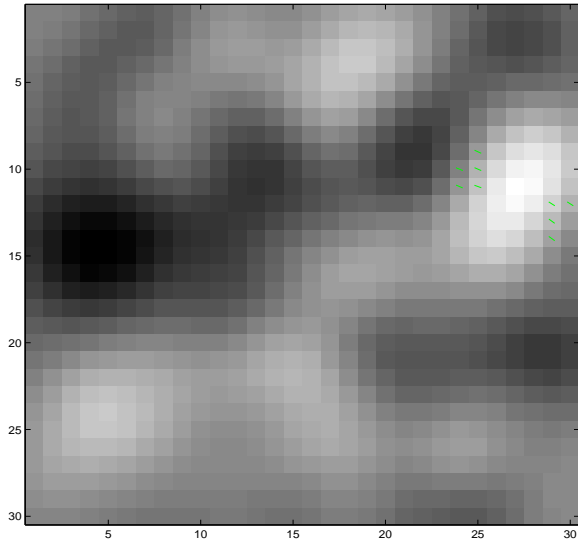


(c) Independent ( $h = 2$ )

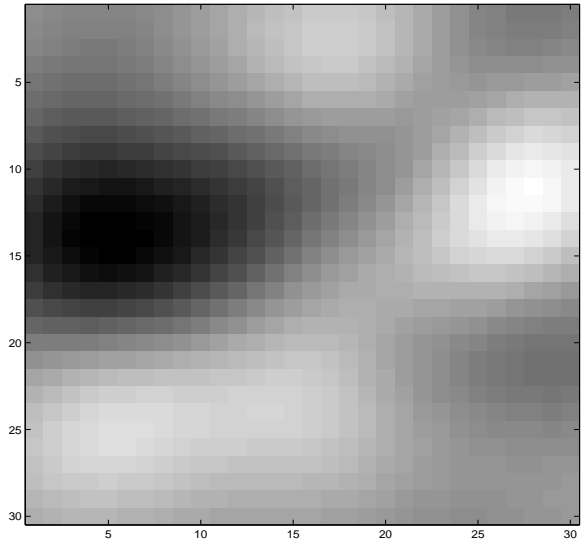


(d) Independent ( $h = 4$ )

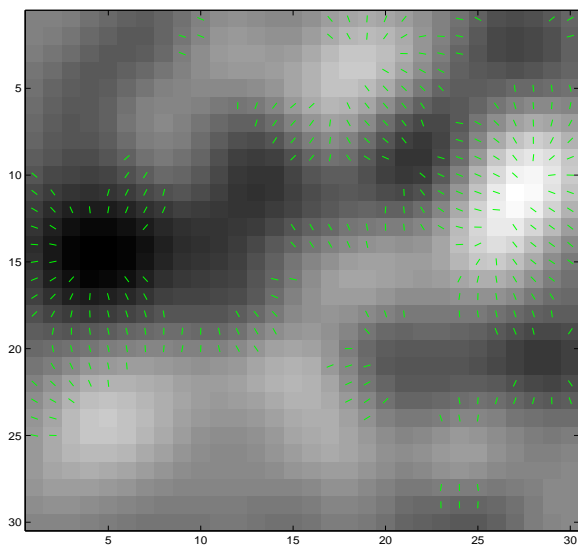
Figure 4: Signal plus Matérn covariance with  $a = 10, b = 5, \nu = 1.5$  on a planar domain



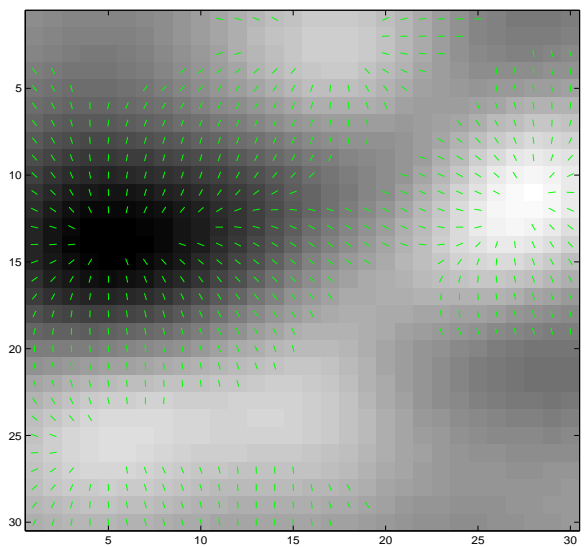
(a) Spatial ( $h = 2$ )



(b) Spatial ( $h = 4$ )

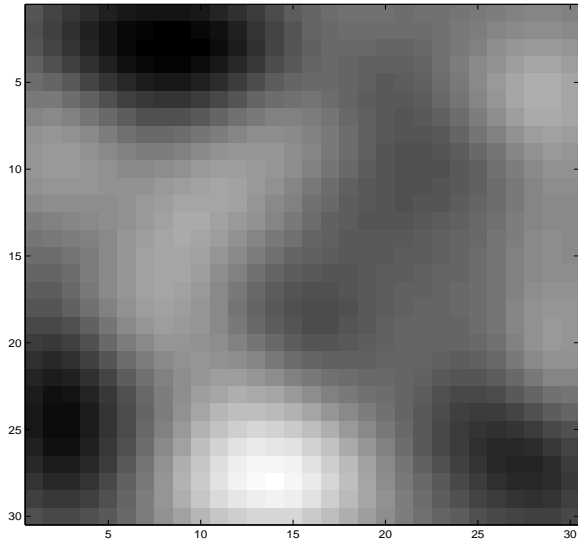


(c) Independent ( $h = 2$ )

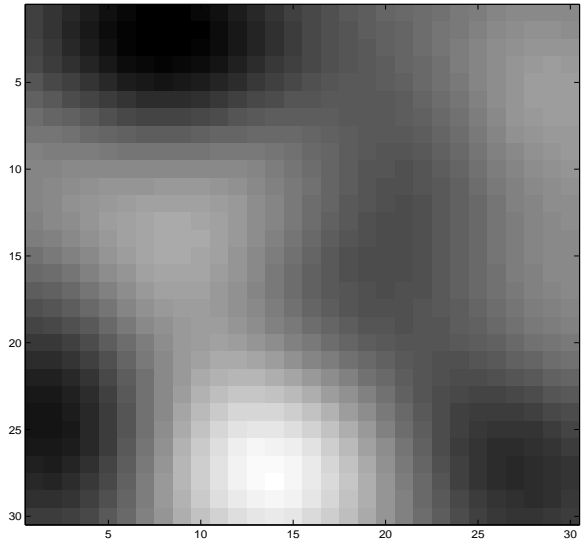


(d) Independent ( $h = 4$ )

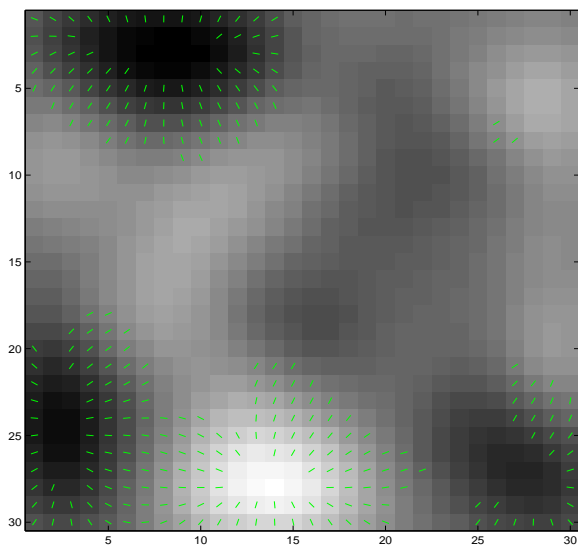
Figure 5: Matérn covariance with  $a = 5, b = 2, \nu = 0.5$  without a signal on a planar domain



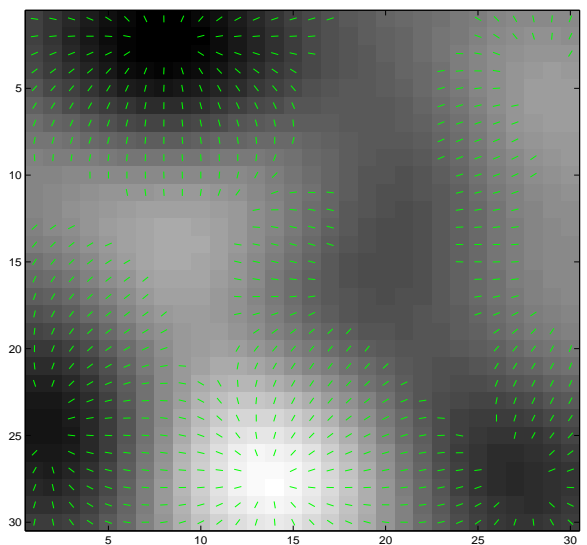
(a) Spatial ( $h = 2$ )



(b) Spatial ( $h = 4$ )

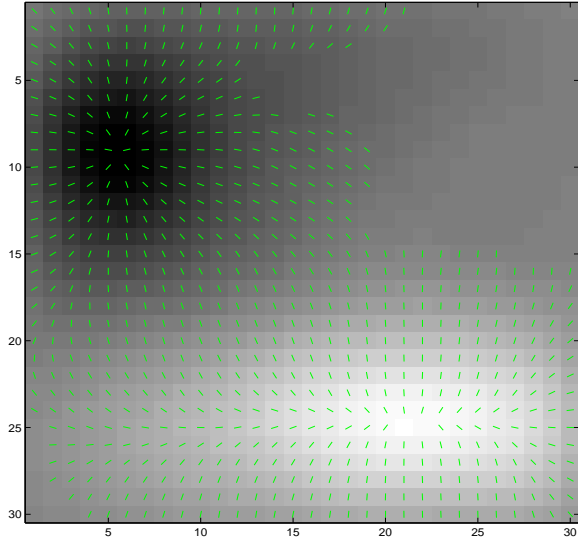


(c) Independent ( $h = 2$ )

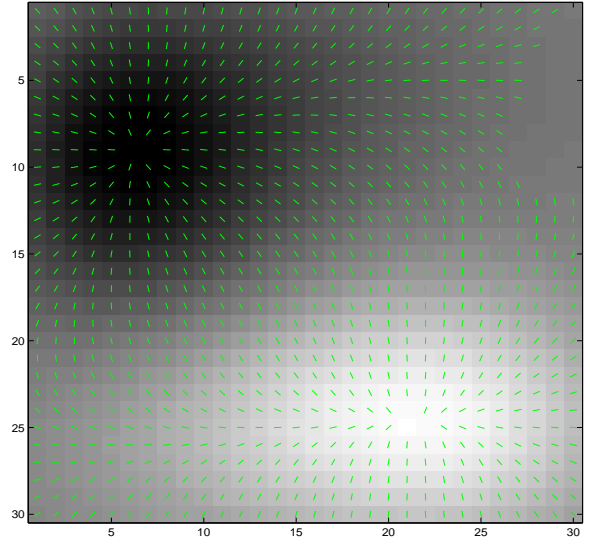


(d) Independent ( $h = 4$ )

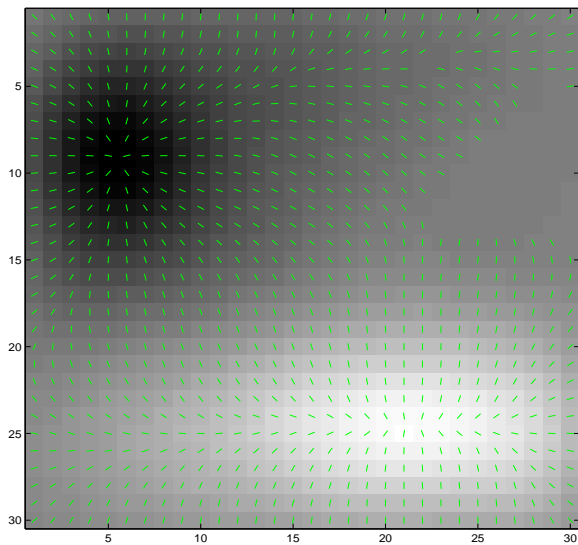
Figure 6: Matérn covariance with  $a = 10, b = 5, \nu = 1.5$  without a signal on a planar domain



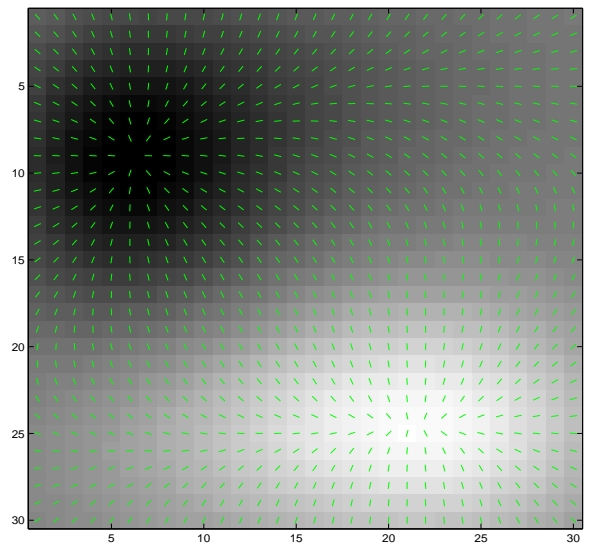
(a) Spatial ( $h = 2$ )



(b) Spatial ( $h = 4$ )

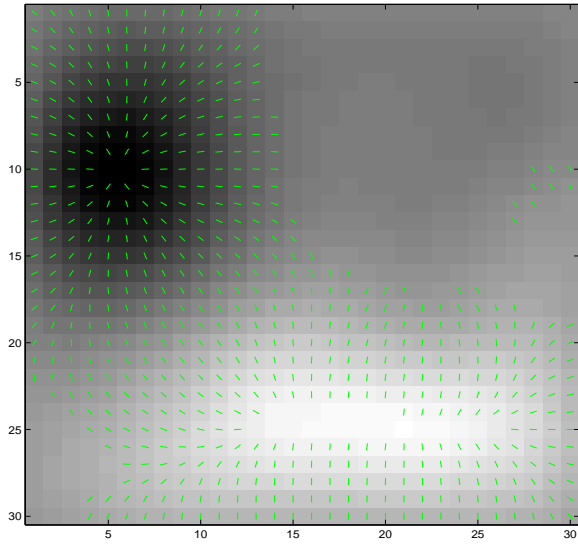


(c) Independent ( $h = 2$ )

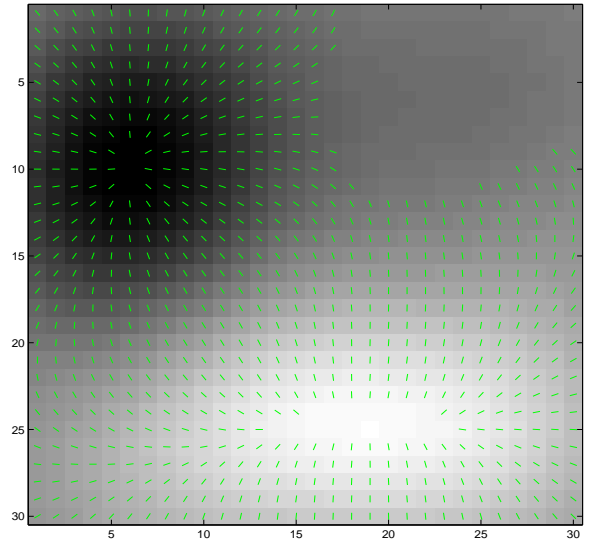


(d) Independent ( $h = 4$ )

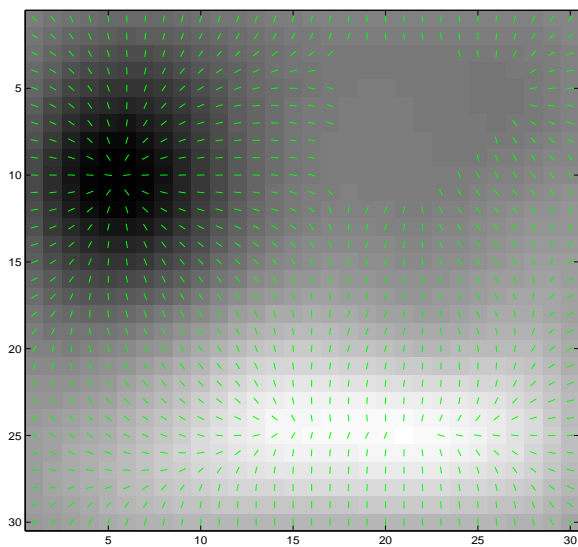
Figure 7: Signal plus Matérn covariance with  $a = 0.03, b = 1000, \nu = 0.5$  in spherical domain



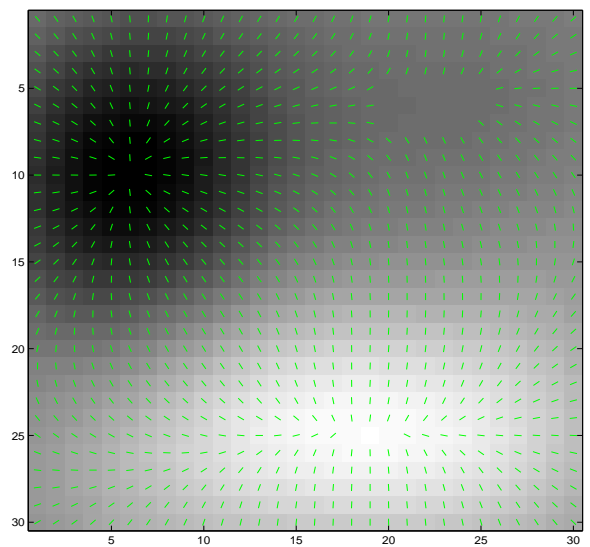
(a) Spatial ( $h = 2$ )



(b) Spatial ( $h = 4$ )

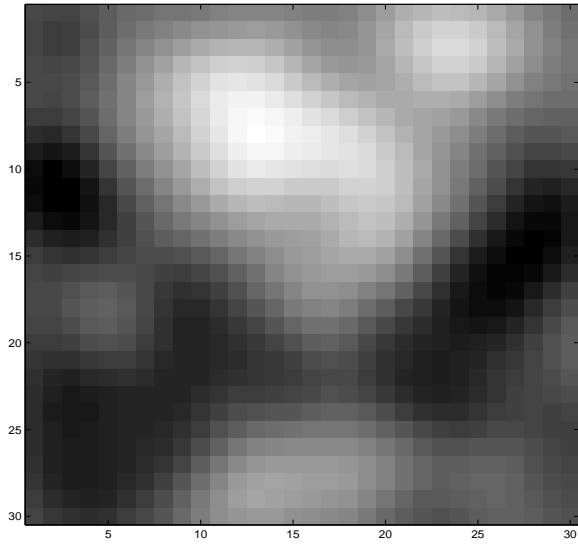


(c) Independent ( $h = 2$ )

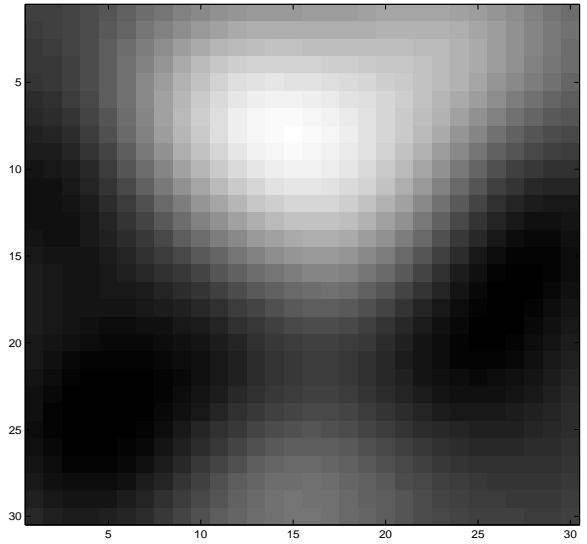


(d) Independent ( $h = 4$ )

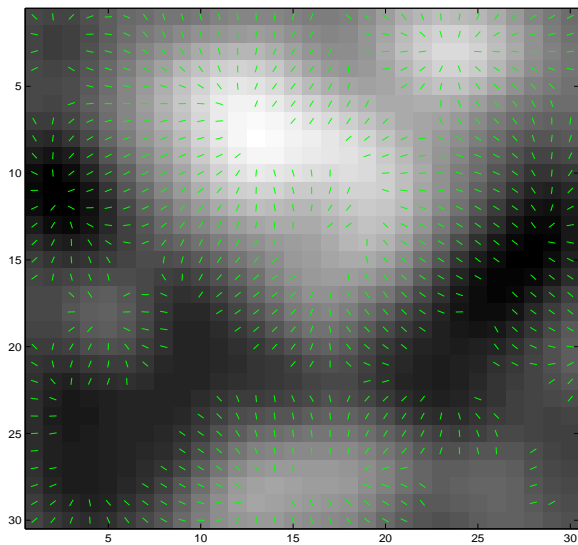
Figure 8: Signal plus Matérn covariance with  $a = 0.08$ ,  $b = 500$ ,  $\nu = 1.5$  in spherical domain



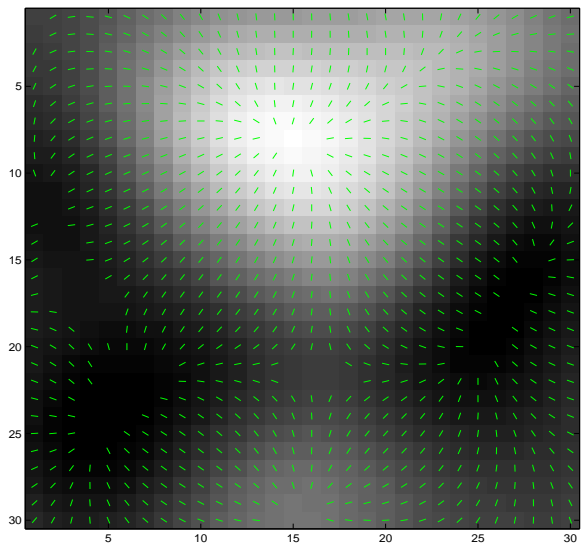
(a) Spatial ( $h = 2$ )



(b) Spatial ( $h = 4$ )

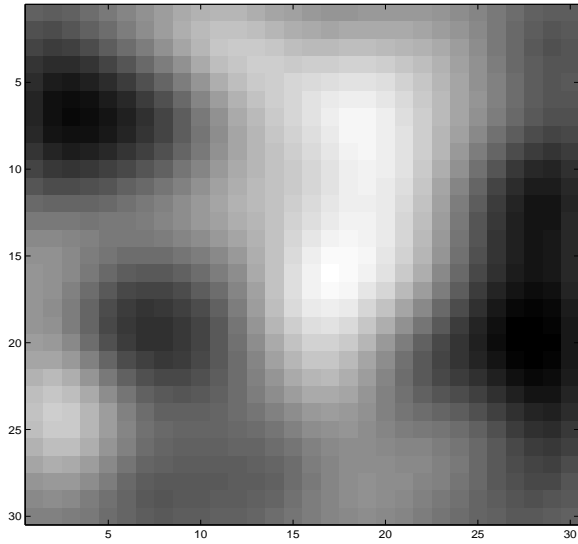


(c) Independent ( $h = 2$ )

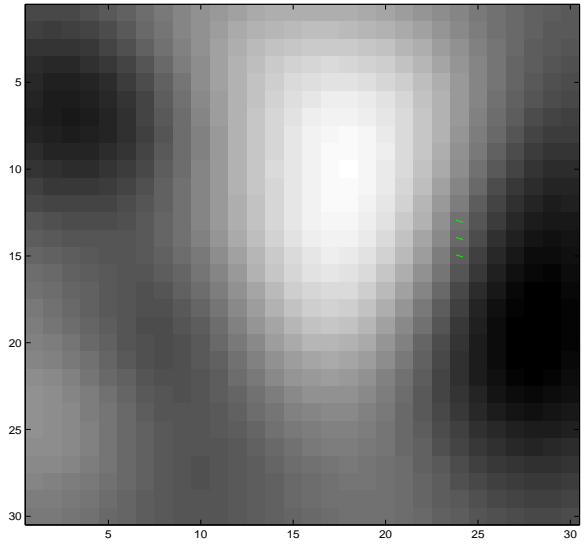


(d) Independent ( $h = 4$ )

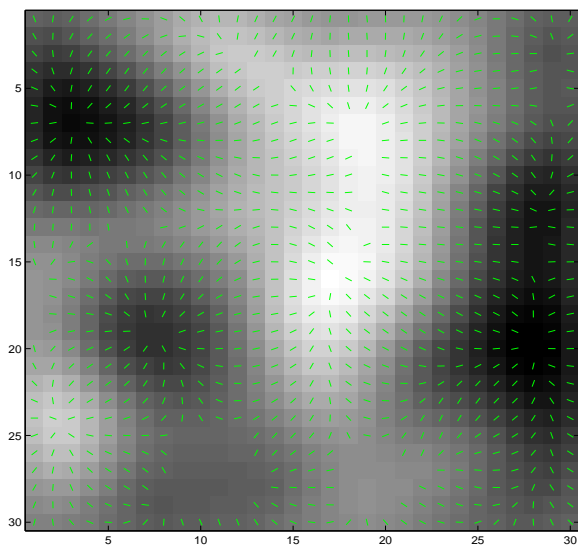
Figure 9: Matérn covariance with  $a = 0.03$ ,  $b = 1000$ ,  $\nu = 0.5$  without a signal in spherical domain



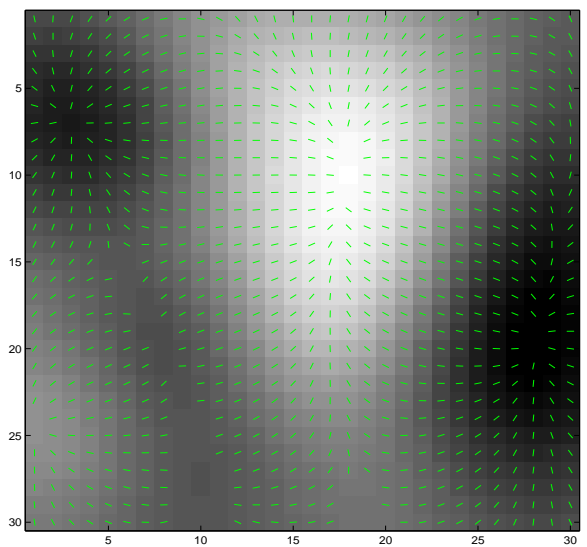
(a) Spatial ( $h = 2$ )



(b) Spatial ( $h = 4$ )

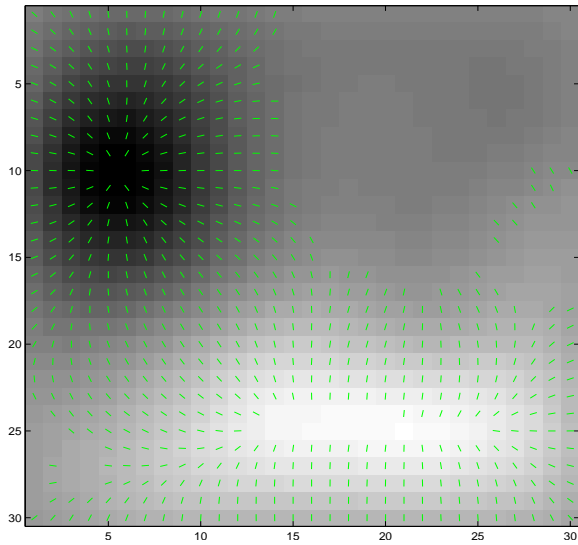


(c) Independent ( $h = 2$ )

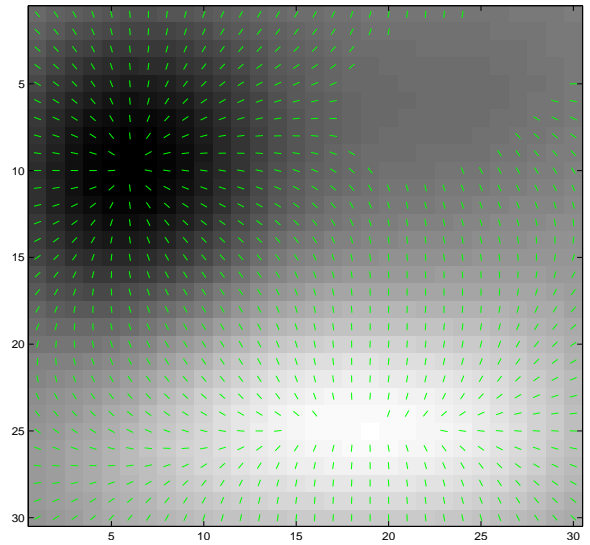


(d) Independent ( $h = 4$ )

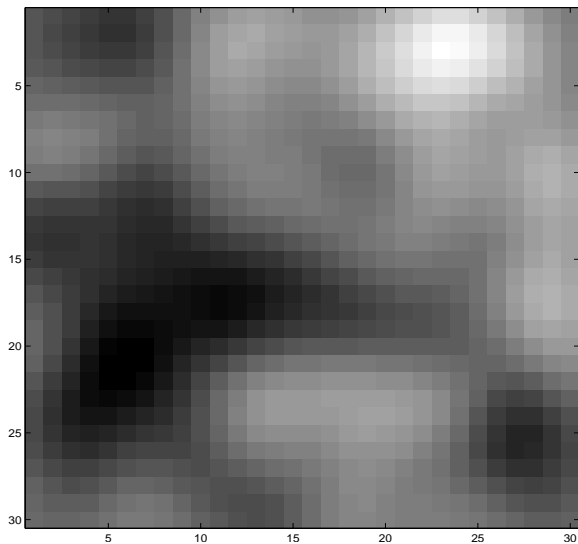
Figure 10: Matérn covariance with  $a = 0.08, b = 500, \nu = 1.5$  without a signal in spherical domain



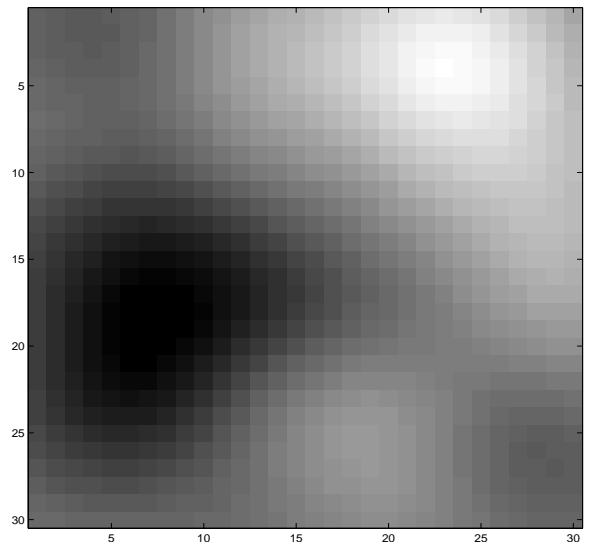
(a) Signal ( $h = 2$ )



(b) Signal ( $h = 4$ )



(c) No signal ( $h = 2$ )



(d) No signal ( $h = 4$ )

Figure 11: The simulated data are generated from Matérn covariance with  $a = 0.08, b = 500, \nu = 1.5$  with and without a signal in spherical domain. In SiZer analysis,  $\nu = 0.5$  is used instead of the true  $\nu = 1.5$ .

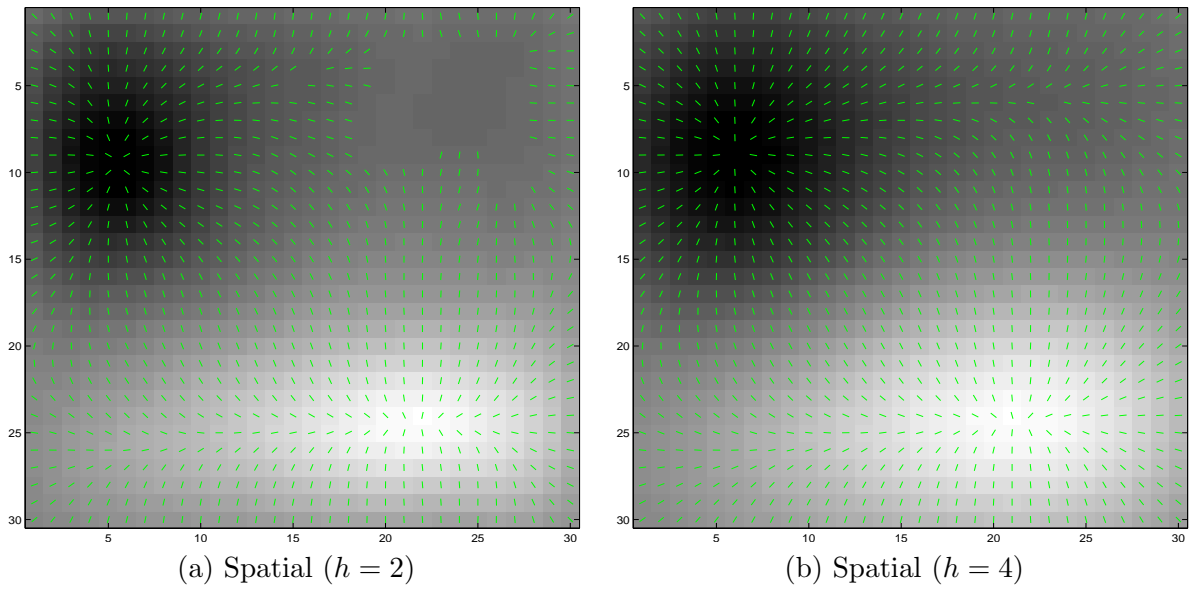
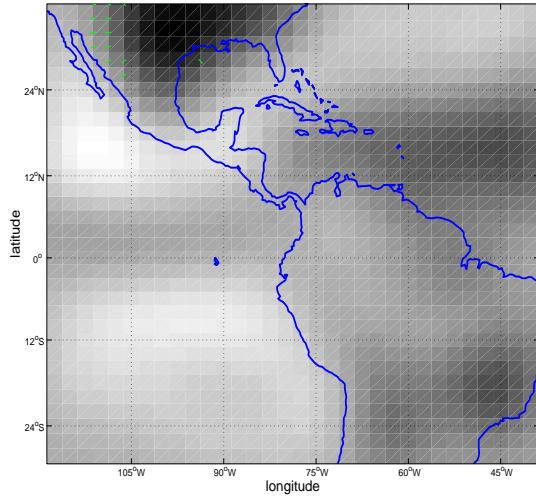
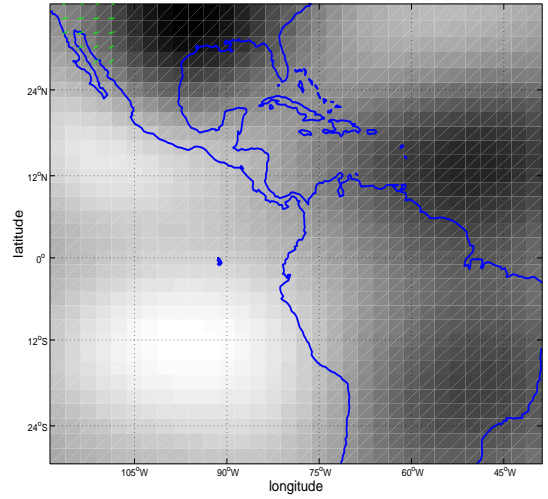


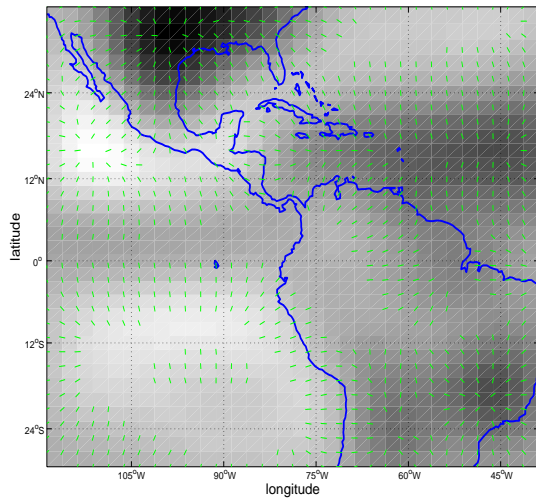
Figure 12: The simulated data are generated from a spherical covariance function with a signal. The spatial SiZer uses the Matérn covariance with  $a = 0.026$ ,  $b = 155.08$ ,  $\nu = 0.87$ .



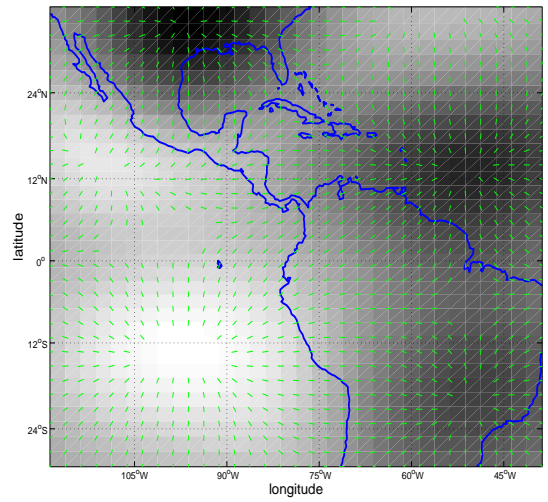
(a) Spatial ( $h = 2$ )



(b) Spatial ( $h = 4$ )

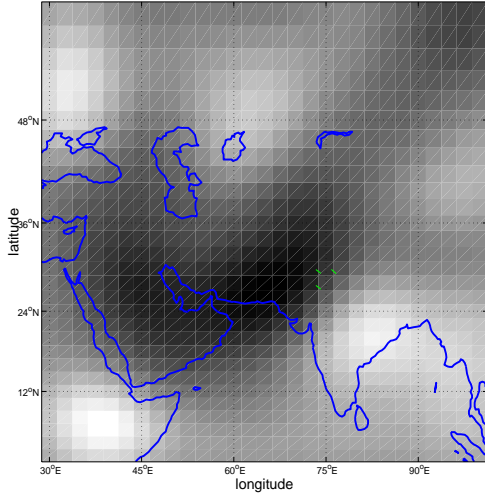


(c) Independent ( $h = 2$ )

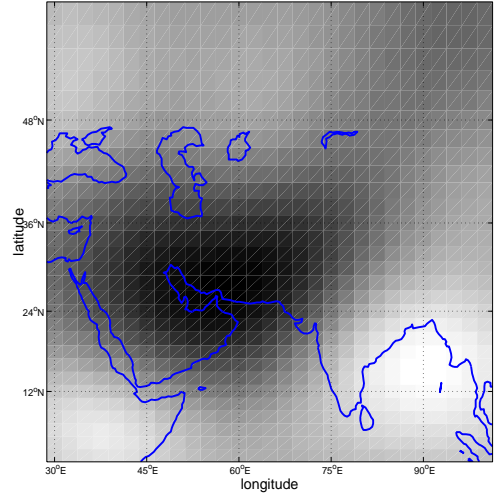


(d) Independent ( $h = 4$ )

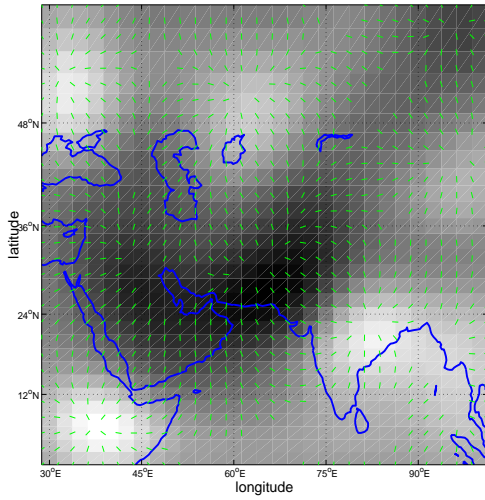
Figure 13: SiZer plots for the North and South America area with the GFDL-CM2.0 model



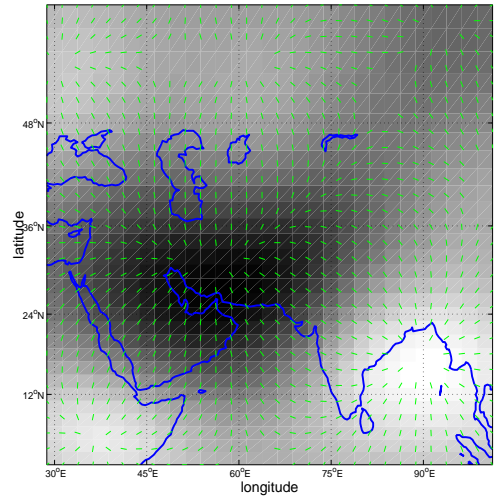
(a) Spatial ( $h = 2$ )



(b) Spatial ( $h = 4$ )

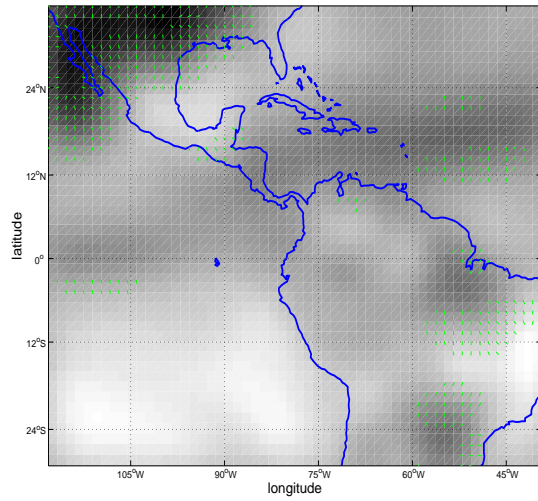


(c) Independent ( $h = 2$ )

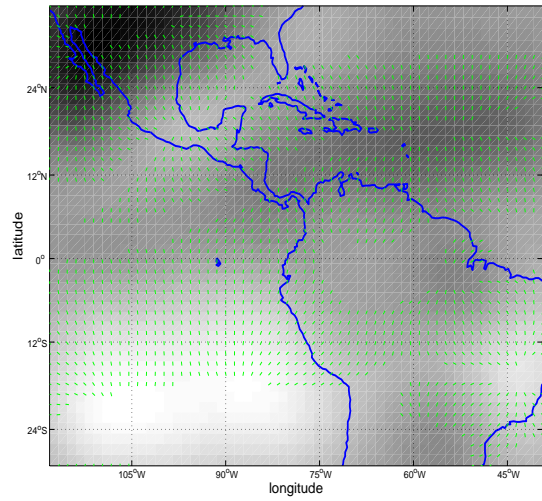


(d) Independent ( $h = 4$ )

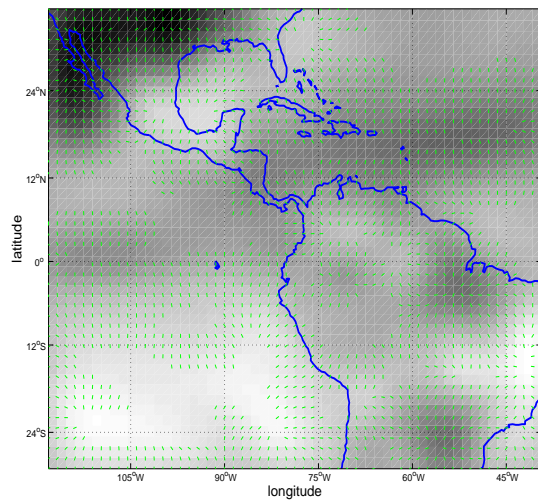
Figure 14: SiZer plots for the Himalayan area with the GFDL-CM2.0 model



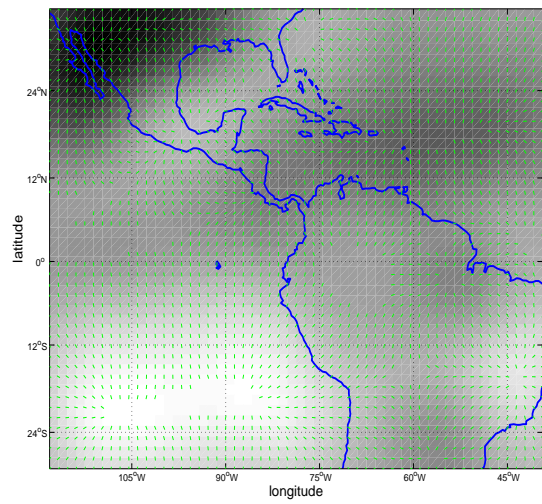
(a) Spatial ( $h = 2$ )



(b) Spatial ( $h = 4$ )

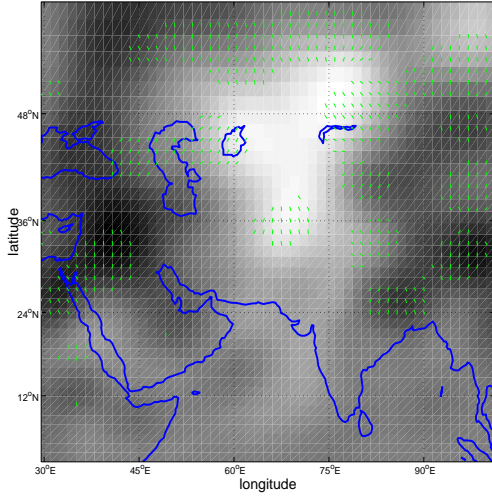


(c) Independent ( $h = 2$ )

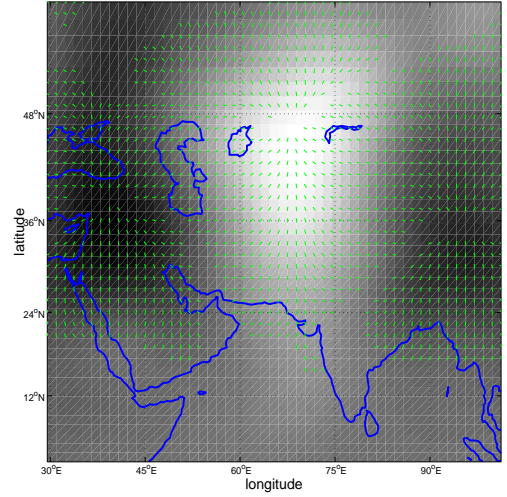


(d) Independent ( $h = 4$ )

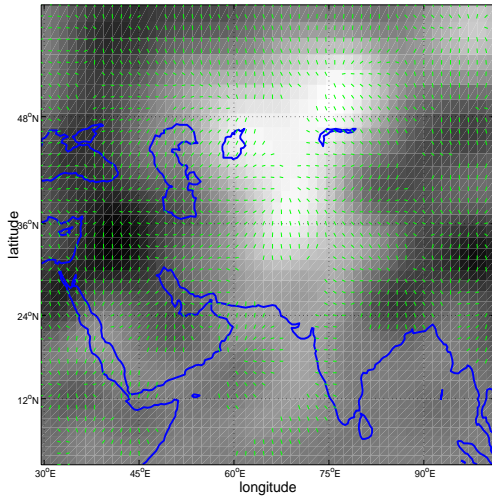
Figure 15: SiZer plots for the North and South America area with the CCSM3 model



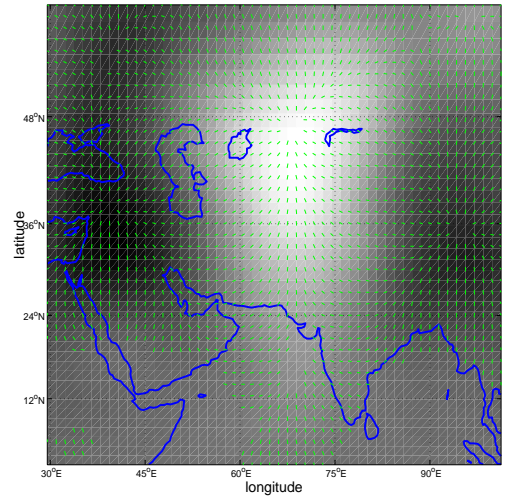
(a) Spatial ( $h = 2$ )



(b) Spatial ( $h = 4$ )



(c) Independent ( $h = 2$ )



(d) Independent ( $h = 4$ )

Figure 16: SiZer plots for the Himalayan area with the CCSM3 model